Composites Part B 173 (2019) 106804

Contents lists available at ScienceDirect

Composites Part B

journal homepage: www.elsevier.com/locate/compositesb

Synthesis of polyaniline-modified graphene oxide for obtaining a high performance epoxy nanocomposite film with excellent UV blocking/ anti-oxidant/ anti-corrosion capabilities

S. Amrollahi, B. Ramezanzadeh, H. Yari *, M. Ramezanzadeh, M. Mahdavian

Department of Surface Coating and Corrosion, Institute for Color Science and Technology, Tehran, 1668814811, Iran

ARTICLE INFO

Keywords:
Polyaniline
Graphene oxide
Epoxy nanocomposites
Weathering
Corrosion

ABSTRACT

This paper focuses on the synthesis and modification of graphene oxide nanosheets with polyaniline. The main aim is to take the advantages of both graphene oxide and polyaniline in enhancing the long-term performance (including weathering and corrosion) of exterior nanocomposites. For this purpose, the synthesized graphene oxide was treated via an in-situ polymerization process. The modified hybrid nanosheets were characterized by Fourier transform infrared spectroscopy (FTIR), Field Emission Scanning Electron Microscopy (FE-SEM), X-ray diffraction analysis (XRD), Ultraviolet–visible spectrophotometry (UV–Vis) and Raman spectroscopy. It was approved that the emeraldine base form of polyaniline has been successfully polymerized on the graphene oxide nanosheets in two forms of non-covalent bonding through π-π interactions between quinoid ring of PANI and basal plane of graphene oxide, and covalent bonding through reaction with epoxide group. The modified nanosheets were introduced into a typical epoxy matrix and then subjected to accelerated weathering and corrosion cycles. The results revealed that a considerable improvement in both weathering (42% reduction in ΔE) and corrosion resistance was achieved which was mainly attributed to the considerable enhancement in UV shielding, radical scavenging as well as better dispersion of graphene oxide modified with polyaniline.

1. Introduction

Organic coatings are applied on the surface to enhance its appearance and to protect the substrate over which they have been applied. Exterior coatings are usually formulated in such a way to withstand the harsh condition of outdoor exposure. Weathering and corrosive factors (i.e. water, sunlight, temperature, etc) are the main destructive environmental influences which not only damage the coating itself, but also cause the coating to malfunction during service life [1,2]. Therefore, it is a high requirement for exterior coatings to be strengthened against weathering and corrosion degradations. Although weathering degradation and corrosion can be logically connected, the mechanisms involved in weathering degradation are different from those of involved in corrosion. These mechanistic differences have led to two independent research areas and weathering and corrosion has been rarely interconnected. The consequence of such independency has resulted in this fact that the strategies implemented against weathering degradation (like addition of organic UV absorbers or inorganic UV-blockers) have not been necessarily in favor of corrosion protection [3–5]. In a similar way, enhancement the corrosion resistance of the coatings (by addition of various corrosion inhibitors or plate-like fillers and etc.) has not led to a considerable improvement in their long-term weathering performance [6,7]. In the recent decade, development of graphene-based materials (thanks to their special structure and properties) has opened a promising window to improve the weathering and corrosion performance of coatings simultaneously [8–10].

Graphene and their derivatives are one-atom thick sheets of carbon with honeycomb-like sp^2 (and sp^3) configuration. Such unique structure has vastly developed the growing application of graphene-based materials in different fields of science and technology [11–15]. Among these various properties, we focus on special characters and properties that can be related to or exploited for weathering and corrosion resistance. The graphene oxide is the oxidized form of graphene. It is dispersed in different media like water much more easily than graphene and can be functionalized for different purposes thanks to its various functional sites available on its surface. Graphene oxide has a band gap of 4.66 ev which can absorb in the high energy part of electromagnetic spectrum (UV radiations mainly in the UV-C and UV-B parts) [16,17].

* Corresponding author.
E-mail address: yari-ho@icrc.ac.ir (H. Yari).

https://doi.org/10.1016/j.compositesb.2019.05.015
Received 8 January 2019; Received in revised form 26 February 2019; Accepted 5 May 2019
Available online 15 May 2019
1359-8368/

Functionalization or reduction of graphene oxide can reduce the band gap energy to 2 ev depending on the nature and the extent of functionalization/reduction. Such reduced band gap causes a red-shift in absorption range, leading to increased absorption in favorable UV-B and UV-A part. Such wide absorption in the harmful part of sunlight (UV-A and UV-B) has attracted the researchers' attentions to the UV shieling properties of graphene-based materials for outdoor applications [18–20]. Another interesting character of graphene-based materials which is highly desired for weathering resistance is their radical scavenging capabilities. Thanking to their electronic structure which contains plenty of delocalized electrons and different functional groups on their surface, graphene and its derivatives can act as electron donor/-acceptor, interacting with various free radical spices generated during photo-degradation [21–23]. It has been demonstrated that such electronic interactions lead to free radical deactivation.

The platelet-like nature is another structural merit of graphene-based materials which can be employed for improving the weathering and corrosion resistance of organic coatings. The high aspect ratio of plate-like graphene and its derivatives enables them to act as physical barrier against water/humidity and corrosive species [24–27]. These nanosheets increase the penetration length and time of water/humidity, oxygen and corrosive species, postponing the hydrolytic degradation or corrosion to much longer times of service life.

Recently, we have exploited these favorable properties to simultaneously enhance the weathering and corrosion resistance of exterior coatings [8,28,29]. We have immobilized organic absorbers and inorganic UV-blockers on graphene oxide nanosheets and achieved considerable improvement in UV shielding and barrier properties [29]. Similarly, in this work, we aim to functionalize graphene oxide with polyaniline via in-situ polymerization process. Composite of graphene oxide and polyaniline has found various applications and its applications are still broadening up [30–35]. We intend to employ this composite structure for improving the weathering and barrier properties of exterior coatings, as its UV shielding properties have been already proved for other applications like fabrics [18–20]. Polyaniline is the most-widely used conducting polymer which has low cost, facile synthesis and high environmental stability. Polyaniline has several desired characters which can be interesting for weathering and corrosion resistance when coupled with graphene oxide nanosheets. Polyaniline exhibits considerable absorption at different regions of electromagnetic spectrum, especially at UV-A range corresponded to the $\pi \rightarrow \pi^*$ transition. Additionally, in situ polymerization of polyaniline in presence of graphene oxide may result in partial reduction of graphene oxide which can cause a favorable red-shift in the UV–Vis absorption spectrum of graphene oxide, as explained before. On the other hands, covering the polar graphene oxide with a layer of polyaniline may provide a more stable dispersion in organic media like polymeric coatings.

Thus, the main target of this work is to combine the advantages of graphene-based materials and polyaniline to achieve a hybrid composite to be further incorporated into an epoxy coating and test its capabilities in simultaneous enhancing weathering and anti-corrosion performance of epoxy coatings.

It should be pointed out that epoxy resin is usually employed as a primer layer in multi-layer coatings and logically, its weathering resistance is not considered at all. But, in some situations the weathering performance of primer layer (epoxy) is so influential on the performance of the whole multi-layer coating system. More details are given in Refs. [36,37].

2. Experimental

2.1. Materials

Steel sheets with thickness of 2 mm, Length and width of 10 cm and 7 cm were supplied from Foolad Mobarakeh Co. Before use, SiC papers with 400, 600 and 800 grits were applied to remove the natural oxide film. Then by acetone, the organic contaminations were carefully removed. Ammonium persulfate, sodium nitrate, hydrogen peroxide and potassium permanganate were purchased from Merck Co. Acids including HCl (37%) and H_2SO_4 (98%) were prepared from Aldrich Co. Aniline and expandable graphite powder were procured from Merck Co., and Kropfmuehl Graphite Co., respectively. Epoxy resin, GZ7 7071X75, and polyamide hardener, CRAYAMID 115, were supplied from Saman and Arkema Co., respectively.

2.2. GO and GO-PANI synthesis methods

Via a modified Hummer's method, discussed in details in our recent works [24,25], the expandable graphite was converted into stable graphene oxide nanosheets (Since after, coded as GO). Conductive polyaniline chains were electrostatically grafted on the GO sheets through a common in-situ oxidative polymerization utilizing ammonium peroxide sulfate as redox initiator [30,38]. For this aim, first, 15 mL HCl solution (1 M) containing aniline (3.2 mM) and ammonium peroxide sulfate (0.8 mM) was prepared and added to 15 mL deionized water solution containing stable dispersion of graphene oxide (25 g/L). The reaction mixture was stirred for 24 h at room temperature (25 ± 3 °C), reaching a dark green mixture which visually confirmed the polyaniline (PANI) deposition on the GO sheets. At the end, the product was filtered and washed for three times with deionized water. The final product was coded as GO-PANI, hereafter.

2.3. Characterization of GO and GO-PANI

FT-IR analysis was applied to characterize the chemistry of GO and GO-PANI by the aid of a PerkinElmer FT-IR instrument. FT-IR spectra were obtained in the range of 4000–400 cm^{-1} wavenumber via a KBr pellet method. The GO and *GO-PANI* crystalline structures were studied by Philips X-ray spectrometer in 5–70° (2θ) range using Cu Kα radiation source (λ = 1.5406 Å). Absorption spectra of aqueous dispersions of GO and GO-PANI were provided by Cecil CE 2021 UV-VIS spectrophotometer. The FE-SEM (Tescan Mira3 LMU) analysis were conducted to study the GO and GO-PANI samples morphology. PANI bonding on the GO sheets was examined by Takram P50C0R10 model (with excitation wavelength of 514 nm) Raman spectroscopy. GO and GO-PANI samples thermal stability was analyzed by STA 1500 by Rheometric Scientific model TGA instrument in nitrogen atmosphere in the range of 25–600 °C with heating rate of 5 °C/min.

2.4. Epoxy/GO and Epoxy/GO-PANI composites preparation

The synthesized nanosheets (GO and GO-PANI) were introduced in a typical solvent-based epoxy resin. The main resin with the commercial name of Araldite GZ7 7071X75 (based on bisphenol A-as 75% solution in xylene, Epoxy equivalent: 600–670 g, viscosity at 25 °C: 8000–13000 m Pa s) was obtained from a domestic supplier (Saba Shimi Aria Co., Iran). The Aqueous GO and GO-PANI were filtered and then, through a solvent exchange process, the particles were dispersed in xylene (the solvent of epoxy resin). The coatings were formulated for 0.1 wt% of nanosheets (GO and GO-PANI) in total formulation. It was then cured with a polyamide-based hardener (CRAYAMID 115, Amine value: 205–220 mg KOH/g, viscosity at 40 °C: around 50000 CPs). The weight ratio of epoxy resin to hardener was 1.3 to 1. Coating samples containing GO and GO-PANI were prepared and coded as Epoxy/GO and Epoxy/GO-PANI, respectively. A blank coating without any graphene oxide was also prepared (coded as Neat Epoxy) and utilized for comparison purpose. All coating samples were applied on steel sheets. The dry film thickness for all coating formulations was adjusted to be 120 μm. The coating curing was performed at ambient temperature for 24 h followed by a thermal curing at 70–80 °C for 4 h.

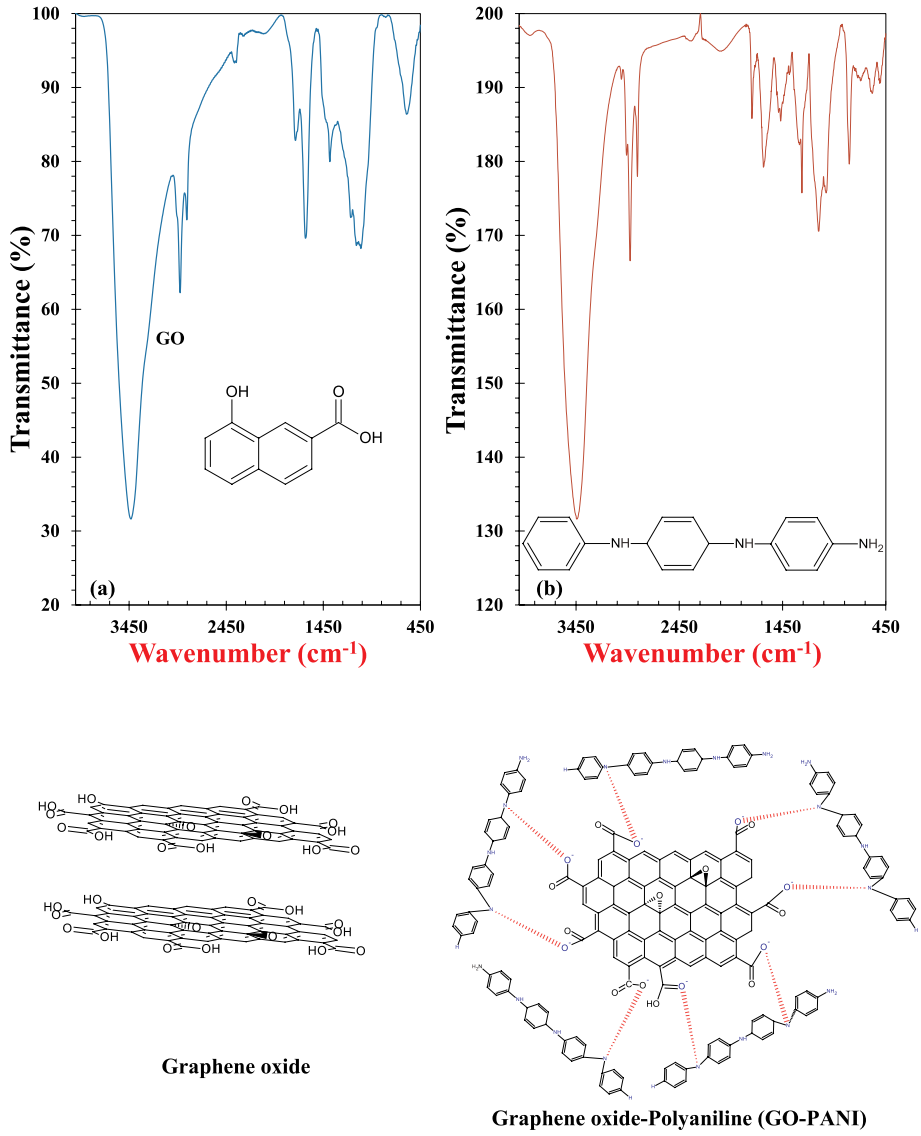

Fig. 1. FT-IR spectra of (a) Neat GO and (b) GO-PANI samples.

2.5. Weathering and corrosion testing of coatings

The prepared coatings were subjected to weathering condition to study the influence of outdoor conditions on various coating properties. For this purpose, a Fluorescent UV-Condensation Type chamber (Model QUV/Basic, Q-Panel Co.) was utilized and set to work according to the ASTM G154. In this standard test method, cyclic exposure to UVA radiation (340 nm, energy of 0.89 W/m^2) at 60 °C for 8 h and condensation condition (100 RH %) at 50 °C for 4 h is applied. The coatings were placed in QUV chamber and removed after pre-determined durations (0, 100, 200 and 300 h) for further characterization.

The weathered samples were characterized with various techniques including colorimetry, contact angle measurements, surface topology and dynamic mechanical thermal analysis. Color of different coatings after various exposure times was measured by a Macbeth CE-741 GL model spectrophotometer. As known, color is multicomponent and has three attributes; L (lightness), a^* (redness–greenness) and b^* (yellowness–blueness). Variations in all three components during weathering and total color difference (ΔE) are usually considered to evaluate the color changes during weathering exposure. ΔE is calculated through the following equation according to CIE 1976 formula [39]:

$$\Delta E = \sqrt{\Delta a^{*2} + \Delta L^{*2} + \Delta b^{*2}} \quad (1)$$

where Delta (Δ) expresses the corresponding difference before and after weathering exposure.

Contact angle measurement was performed to study changes in the surface hydrophilicity of the coatings. The contact angle measuring system used was a Data physics OCA15 plus instrument. Distilled water was employed as probe liquid and average of five measurements was calculated and reported. Surface topology of different coatings was also observed by an atomic force microscope (AFM) instrument (DME scanner DS 95–50).

The structural and thermo-mechanical properties of different coatings after curing and weathering processes were studied by dynamic mechanical thermal analysis (DMTA). It was performed by means of a Teritec 2000 instrument. Each DMTA experiment was carried out at 1 Hz and the temperature was scanned from 30 to 160 °C with a heating rate of 10 °C/min.

Utilizing Ag/AgCl (Sat.), graphite wire and coated steel sample respectively as reference, auxiliary and working electrodes in an electrochemical cell, the anti-corrosion properties of the coated samples were compared before and after QUV exposure by Ivium Compactstat

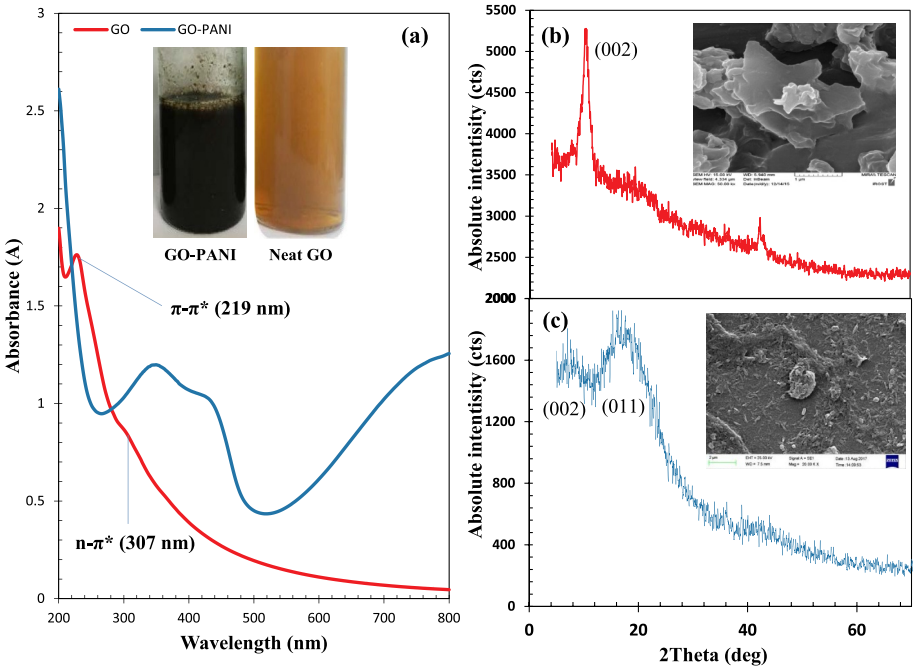

Fig. 2. (a) UV–Visible spectra and XRD patterns and SEM images of (b) Neat GO and (c) GO-PANI samples.

EIS. This analysis was conducted on 1 cm^2 of the coated samples immersed in 3.5 wt% chloride solution in a 10 mHz-10 kHz frequency range under open circuit potential (OCP), where 10 mV peak to zero amplitude sinusoidal voltage was employed. Accelerated corrosion test was done according to ASTM B117 through exposing the scratched samples to salt spray condition (5% NaCl fog, pH: 7, temperature: 35 °C).

3. Results and discussion

3.1. GO-PANI characterization

According to FT-IR spectrum of GO (Fig. 1), the main peaks located at 1643 cm^{-1} and 1751 cm^{-1} are corresponded to the C=C and C=O bands stretching vibrations, respectively [30,40,41]. The O–H deformation in COOH group can be seen at 3450 cm^{-1}. The absorption band associated with C–O stretching in epoxide group (C–O–C) appeared at 1118 cm^{-1}. The PANI deposition on the GO sheets can be perceived from the observation of absorption peaks at 1494 cm^{-1} and 1642 cm^{-1} which are associated with the C=C bands stretching vibration of the quinonoid and benzenoid units. In addition, appearance of C–N band stretching at 1304 cm^{-1} can approve covalent bonding of polyaniline on graphene oxide nanosheets through reaction with epoxide ring existed on the basal plane of GO [42].

UV–Visible spectra corresponded to the absorption of aqueous extract of GO and GO-PANI are depicted in Fig. 2a. UV–Visible absorption spectrum of neat GO exhibits two peaks; a strong and sharp absorption peak at 219 nm and a less intensive peak around 307 nm, which are related to the electron orbital transition of π–π* (aromatic C=C bonds) and n-π* transition related to carbonyl (C=O) groups [43]. According to Fig. 2, the peak corresponded to the transition of π–π* is almost disappeared, indicating the thick PANI layer deposition over the GO sheets, weakening the benzene rings absorption. The peaks observed in the wavelength range of 300–500 nm are the polaronic transition (polaron–π*), corresponded to the PANI molecules bonded with GO sheets [44].

XRD patterns of GO and GO-PANI are provided in Fig. 2b. Only one intensive peak centered at $2\Theta = 10.25$ (002) can be seen in the diffraction pattern of neat GO. PANI bonding with GO sheets shifted the major (002) peak related to GO to $2\Theta = 6.12°$, confirming the PANI role in GO interlayer space increment. The sharp and broad diffraction peak (011) located at $2\Theta = 16.29°$ in the XRD pattern of GO-PANI is related to the PANI chains grafted on the GO sheets [45,46].

SEM images presented in Fig. 2 declared that the multilayered GO sheets are in aggregated form and have wrinkled structure but the PANI deposition on the GO sheets significantly changed the morphology. The layered structure of GO is not visible anymore after PANI deposition, indicating the PANI film role in particles agglomeration prevention.

Raman spectroscopy results for two samples of GO and GO-PANI are presented in Fig. 3 Two characteristic D- and G-Bands, which are respectively associated with the density of defects within GO sheets and the sp^2 bonded carbon bonds of the graphitic sheets, are centered at 1350 and 1586 cm^{-1} wavenumbers. The PANI deposition on the GO sheets can be evidenced from the observation of absorption bands centered at 1165 cm^{-1} (C–H bending of the quinoid benzenoid ring), 1323 cm^{-1} (C–C stretching vibration of quinoid rings), 1461 cm^{-1} (C–N stretching band of quinoid rings) and 1560 cm^{-1} (C–C stretching vibration of benzenoid). The red shift associated with the D-band from 1350 cm^{-1} to 1333 cm^{-1} for GO-PANI compared with GO evidences the π-π interactions between the quinoid ring of PANI and graphene oxide sheets [47,48]. Results show that after PANI deposition on the GO sheets the 2D band intensity decreased, revealing that there is more than one layer of graphene sheets and the success of GO reduction by PANI.

TGA/DTG analysis was carried out to study the influence of PANI chains grafting (covalent/non-covalent) on GO thermal stability (Fig. 4). DTG plot of GO depicts four major mass loss steps in the temperature zones of (I) 100–120 °C, (II) 120–180 °C, (III) 180–320 °C and (IV) 420–600 °C, which are respectively assigned to the removal of water molecules physically adsorbed on the GO surface (Zone I), decomposition of less thermal stable oxygen-functional groups (like O–H) (Zone II), decomposition of more stable oxygen-functional groups (like epoxide and carboxylic groups) (Zone III)and pyrolysis of GO carbon skeleton (Zone IV) [49,50]. The remained weight at 600 °C for GO is about 13.4%. On the other hand, there is no obvious significant weight loss step up to 340 °C in the TGA/DTG plots related to GO sheets modified by PANI. This result evidences that PANI chains grafting onto GO sheets could promote the GO sheets thermal stability through interactions with oxygenated-functional groups. Above 340 °C with increasing the temperature a significant decreasing trend for weight can be seen, noting the

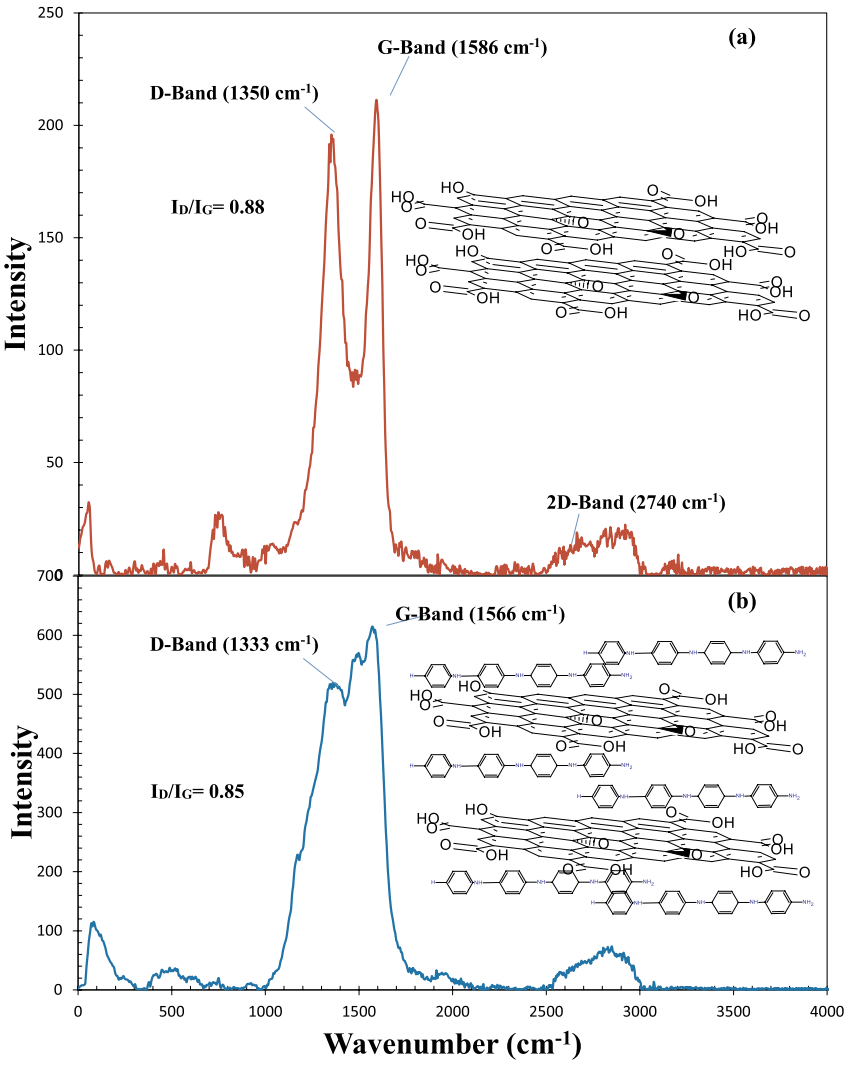

Fig. 3. Raman spectra of (a) Neat GO and (b) GO-PANI samples.

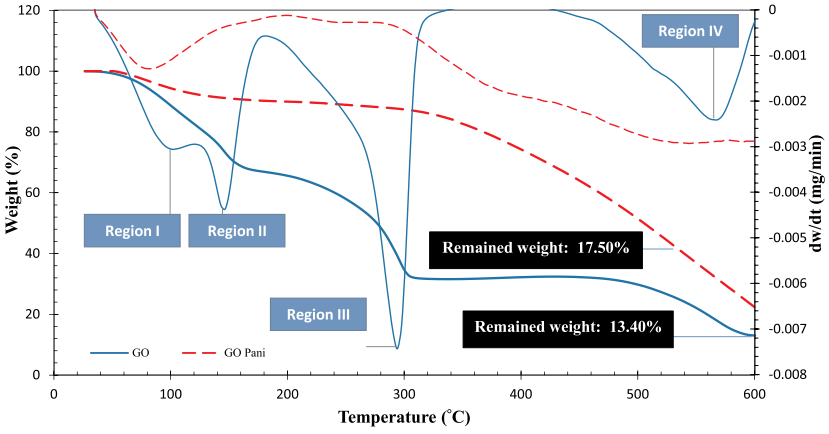

Fig. 4. TGA and DTG plots of GO and GO-PANI nanosheets.

PANI chains decomposition [51,52]. The remained weight at 600 °C for PANI modified GO is about 17.5%. TGA results clearly evidenced that PANI chains adsorption onto GO could promote its thermal stability.

In order to assess the antioxidant capability of synthesized GO and GO-PANI nanosheets, the DPPH assay was conducted on the samples. The inhibition performance of GO and GO/PANI samples are plotted in Fig. 5, as diagrams of the inhibition versus concentration.

The results clearly demonstrate that GO and GO-PANI nanosheets present different level of inhibition. While the GO exhibits a low level of inhibition even at high concentrations, GO-PANI composite efficiently

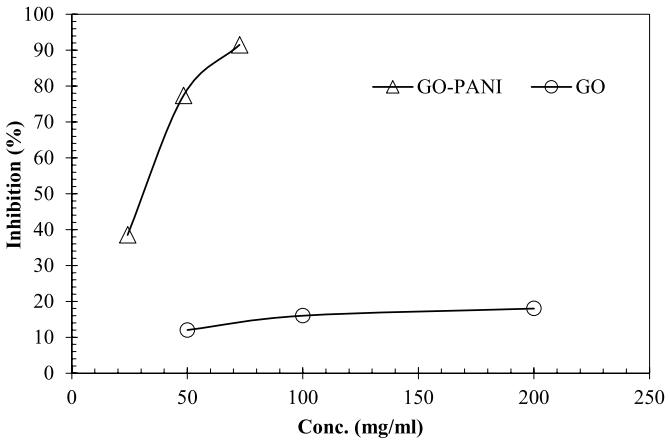

Fig. 5. The inhibition (%) versus concentration for GO-PANI nanosheets.

scavenges the DPPH radicals at much lower concentrations compared to GO. Such different behavior in radical scavenging is quantified in term of IC50. The IC50 values for the synthesized GO and GO/PANI are 1.04 and 0.034 mg, respectively. According to the IC50 definition, the lower IC50 indicates the higher inhibition and radical scavenging capability. Thus, a great reduction in IC50 value after modification of GO by polyaniline can be an efficient treatment to considerably improve the radical scavenging characteristic of graphene oxide. The enhanced radical scavenging properties of GO-PANI can be a promising for promoting the long-term properties of the polymeric systems in which they are incorporated.

3.2. Weathering performance of filled coatings

So far, the deposition of PANI over graphene oxide was approved with various techniques. As stated earlier, the synthesized GO and GO-PANI were incorporated into epoxy and then exposed to cyclic weathering and corrosion tests. The weathering and corrosion performance of the filled coatings after various time of exposure was evaluated by different techniques.

3.2.1. Visual properties

The coating appearance especially its color is the first visual attribute which is affected during weathering. Thus, the color changes of different coatings (neat, GO- and GO-PANI-filled epoxy) was studied by the extent of variations in their color attributes (L*, a*, b*) during weathering exposure. Our results revealed that among different color attributes, the most variations occurred in b* and L*. Therefore, the color changes after weathering are presented in terms of Δb*, ΔL* and ΔE (the total color change) in Fig. 6.

As known, the major color component which is generally considered in weathering performance is variations in blueness-yellowness (Δb) of sample. As can be seen in Fig. 6, Δb for Neat Epoxy demonstrates the highest changes. Positive Δb after weathering means an increase in absorption of violet/blue wavelengths, turning the sample yellow. This color change is mainly attributed to the formation/growth of chromophoric species on the polymeric chains as a results of photo-degradation [53,54]. Addition of graphene oxide into coating has resulted in a considerable drop in Δb. A much further drop in Δb is observed when GO-PANI is incorporated into the epoxy coating. The lowest changes in Δb for GO-PANI/Epoxy implies to the lowest accumulation amount of photo-degradation products during weathering.

The similar trend of variations is seen for ΔL. The decrease in lightness is mainly due to the decrease in smoothness of the coating surface which deviates the incident light, leading to lower amount of perceived lightness.

ΔE as the total color change which is the sum of variations in all color components (L*, a*, b*) is seen in Fig. 6. According to this Figure, Neat Epoxy sample demonstrates the highest ΔE after 300 h weathering exposure. The higher ΔE means the higher level of color variations during exposure, representing the lower weathering stability. By addition of graphene oxide into epoxy, ΔE decreases which reveals a higher level of weathering stability in presence of graphene oxide nanoplatelets. For the GO-PANI/Epoxy sample, the least changes in ΔE is observed.

The lowest variations in main color parameters (Δb, ΔL and ΔE) for

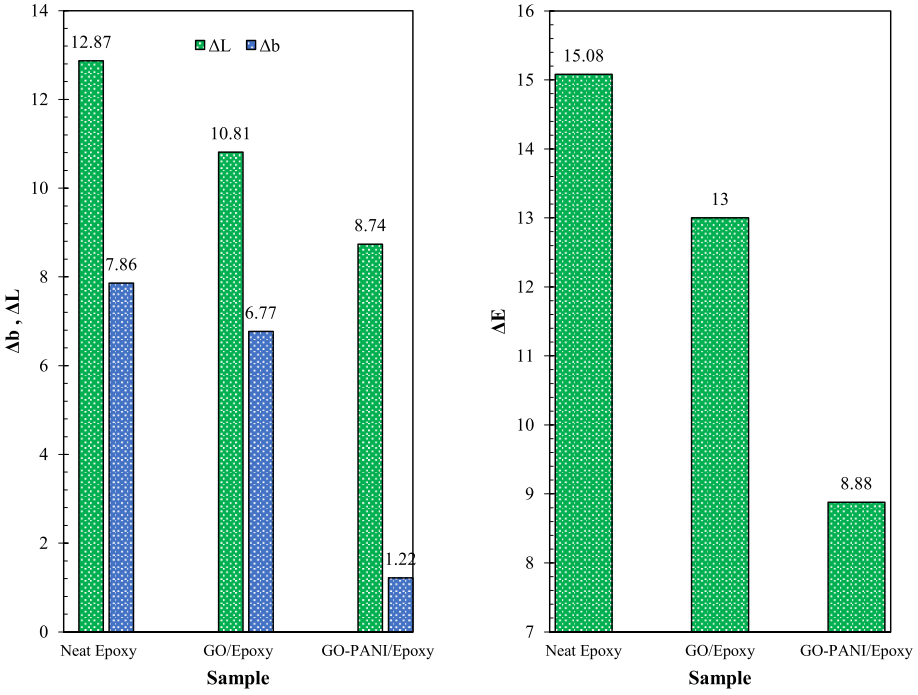

Fig. 6. The variations in ΔL, Δb, and total color change (ΔE) for different samples after weathering exposure. (For interpretation of the references to color in this figure legend, the reader is referred to the Web version of this article.)

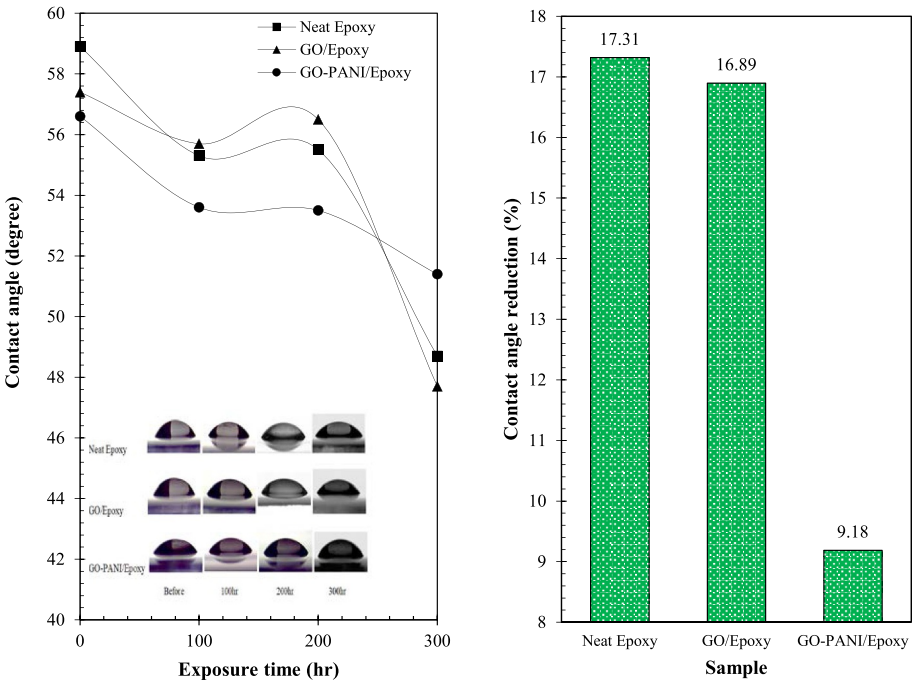

Fig. 7. Changes of water contact angle against exposure time and its reduction percentage for different coatings.

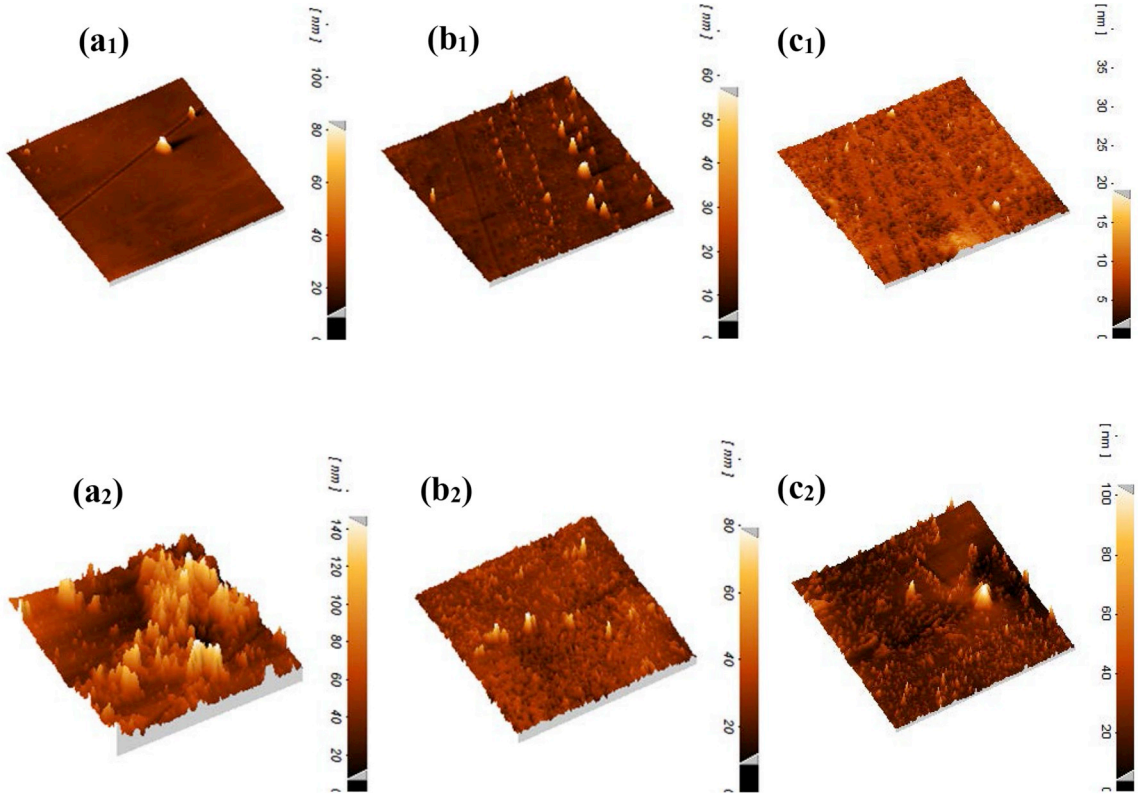

Fig. 8. 3D AFM images of Neat Epoxy (a1.a2)GO/Epoxy (b1,b2) and GO-PANI/Epoxy(c1,c2) samples(subscripts 1 and 2 respectively refer to before and after 300 h weathering).

GO-PANI/Epoxy sample after weathering can clearly reflect the highest level of weathering protection in presence of graphene oxide modified with polyaniline.

3.2.2. *Surface properties*

The surface character of the coatings was studied by the aid of contact angle measurements before and after weathering exposure. Fig. 7 shows the variations in water contact angle for different coatings during weathering.

Table 1
Roughness values before and after weathering time (0, 300 h).

AFM									
	S_a (nm)			Sz (nm)			S_q (nm)		
	Before	After	difference	Before	After	difference	Before	After	difference
Neat Epoxy	1.52	13.25	11.73	29.56	120.03	90.47	2.42	18.91	16.49
GO/Epoxy	3.03	4.72	1.69	54.91	90.98	36.07	4.53	7.50	2.97
GO-PANI/Epoxy	1.35	4.05	2.7	29.47	69.48	40.01	2.04	6.98	4.94

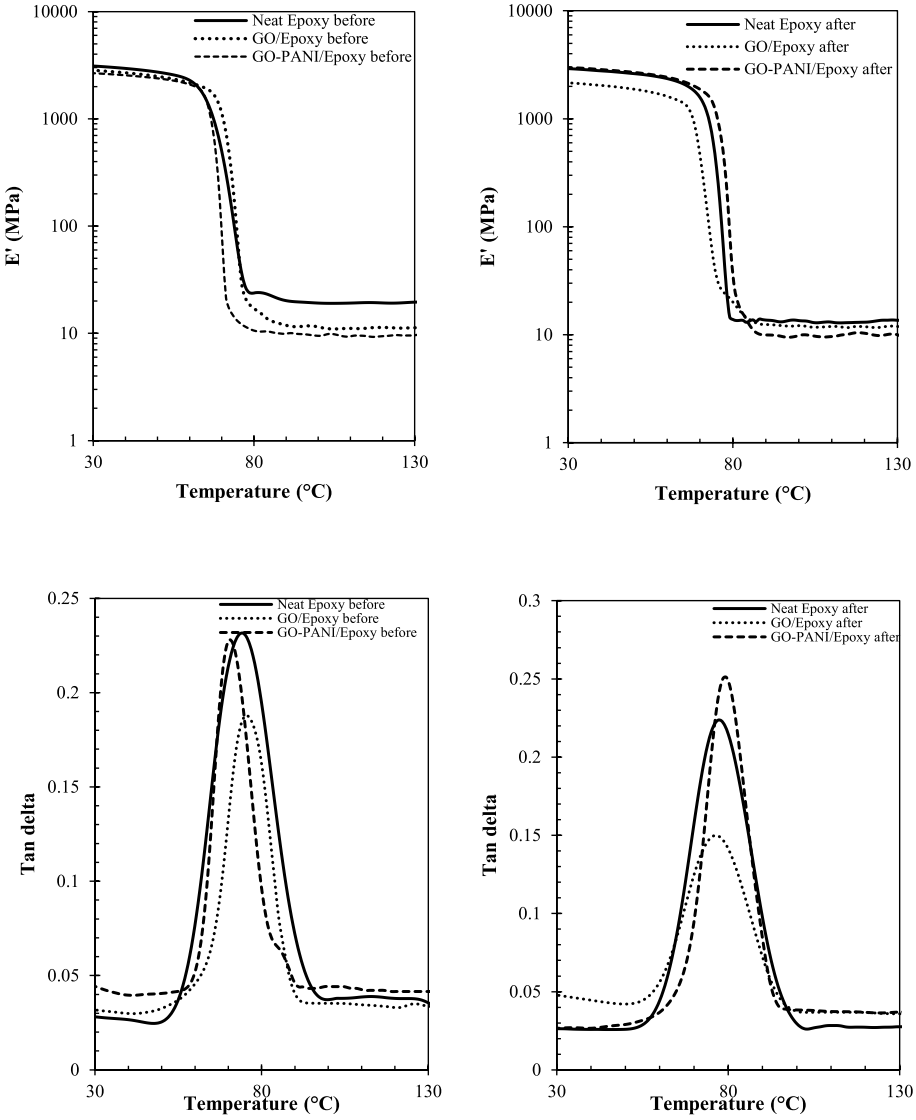

Fig. 9. Storage modulus and Tan delta diagrams for different coatings before and after 300 h weathering exposure time.

The results in Fig. 7 demonstrate that before being exposed to weathering condition, the highest water contact angle belongs to the Neat Epoxy sample. It can also be seen that modification of coating with neat GO and GO-PANI lead to a slight decrease in water contact angle. Such results reveal that both GO and GO-PANI fillers have a slight influence on increasing the hydrophilicity of the surface. The polar nature of graphene oxide which accommodates several polar groups like hydroxyl, carboxylic acid, epoxides on its surface seems to be the plausible reason of such increased hydrophilicity for GO/Epoxy specimen. Additionally, it is observed that further hydrophilic character of GO-PANI/epoxy compared to GO/epoxy may be assigned to the polar nature of polyaniline which contributes in surface free energy and contact angle.

Fig. 7 obviously demonstrates that as weathering proceeds, water contact angle gradually decreases, denoting an increase in surface hydrophilicity during weathering. It is well-known that increased hydrophilicity during weathering is an indicative of weathering stability [55]. As the weathering time elapses, the degradation products (which are usually polar species) accumulate on the coating surface, leading to increased hydrophilicity. Therefore, the amount of water contact angle reduction can be an indicator for weathering stability. Fig. 7 also presents the value of water contact angle reduction (in percentage) for different coatings after being exposed to weathering for 300 h.

It can be seen from Fig. 6 that the contact angle reduction (%) for Neat epoxy, GO/epoxy and GO-PANI/Epoxy specimens are respectively

Table 2
Crosslink density, Tg, and peak width of different coatings deduced from DMTA diagrams.

	Crosslink density (mol/m3)		T_g(°C)		Peak width(°C)	
	Before	After	Before	After	Before	After
Neat Epoxy	2061.74	1450.41	74.1	77.4	20	21
GO/Epoxy	1164.07	1242.69	75.5	76.4	14	20
GO-PANI/Epoxy	1015.75	1063.69	70.5	78.9	12	14

17, 16 and 9%. This indicates that both GO/epoxy and GO-PANI/Epoxy samples have protected their surface during weathering more efficiently than Neat epoxy. Such maintenance is much more efficient in case of GO-PANI/epoxy. These results clearly point out that modification of graphene oxide with polyaniline has a considerable effect on the surface protection of the coating. Such modification seems to be influential on protecting the surface against chemical and topological changes. This protection has led to less formation/growth of polar products of weathering degradation (chemically) and probable the more intact surface of epoxy coating (topologically). The surface morphology of various epoxy coatings was studied before and after weathering by Atomic force microscopy (AFM) technique. Fig. 8 depicts the AFM micrographs of different coatings before and after weathering exposure for 300 h.

The AFM micrographs (Fig. 8) can be quantified by various terms. The roughness parameters including S_a (average roughness), S_q (root mean square roughness) and S_z (10-point height average of valleys/summits difference) are reported in Table 1. As observed in Fig. 8 and Table 1, before weathering, the Neat Epoxy specimen has a relatively smooth surface. It is also demonstrated that the surface roughness considerably increases after addition of graphene oxide. The increment in surface roughness can be logically due to the addition of high aspect ratio graphene oxide nanoplatelets into coating. Surprisingly, it is observed that, before exposure, GO-PANI/Epoxy sample has a smooth surface, as smooth as neat epoxy. It seems that presence of polyaniline layer over graphene oxide has increased the compatibility of graphene oxide with epoxy matrix. Such improved compatibility can increase the uniformity and homogeneity of the composite, forming a smoother surface. After weathering, the surface roughness of all specimens increases which is because of surface degradation in weathering cycles. In weathering degradation, polymeric chains are gradually broken to water soluble products and lower molecular weight chains which can be released from the coating, leaving unevenness on the surface [56–59]. Considering AFM micrographs and roughness parameters after weathering shows that while Neat Epoxy experiences the highest rate of changes in roughness parameters, both GO/Epoxy and GO-PANI/Epoxy specimens endure slight changes which is again an indication of their high level of protection against humidity and UV exposure. The smoothest surface after 300 h accelerated weathering belongs to the

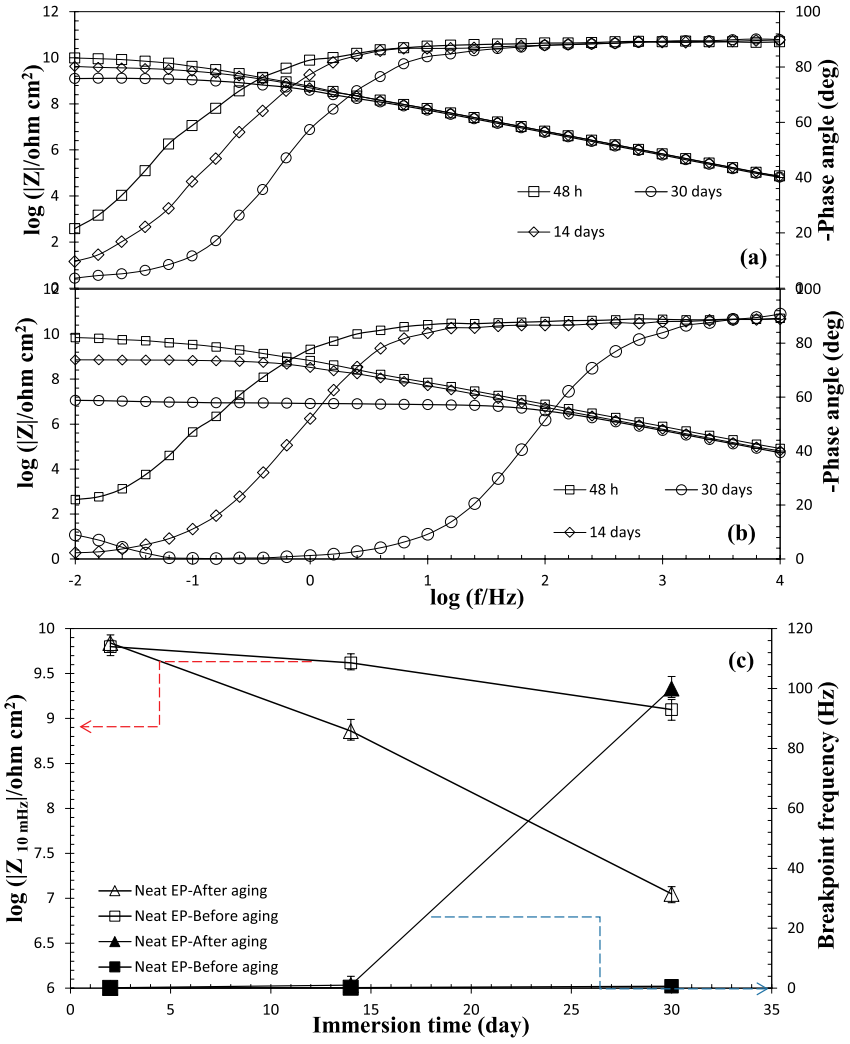

Fig. 10. Bode diagrams of Neat epoxy samples exposed to 3.5 wt% NaCl solution for 30 days, (a) before QUV aging and (b) after 300 h QUV aging; (c) the plots of Z10 mHz and breakpoint frequency versus the time of immersion.

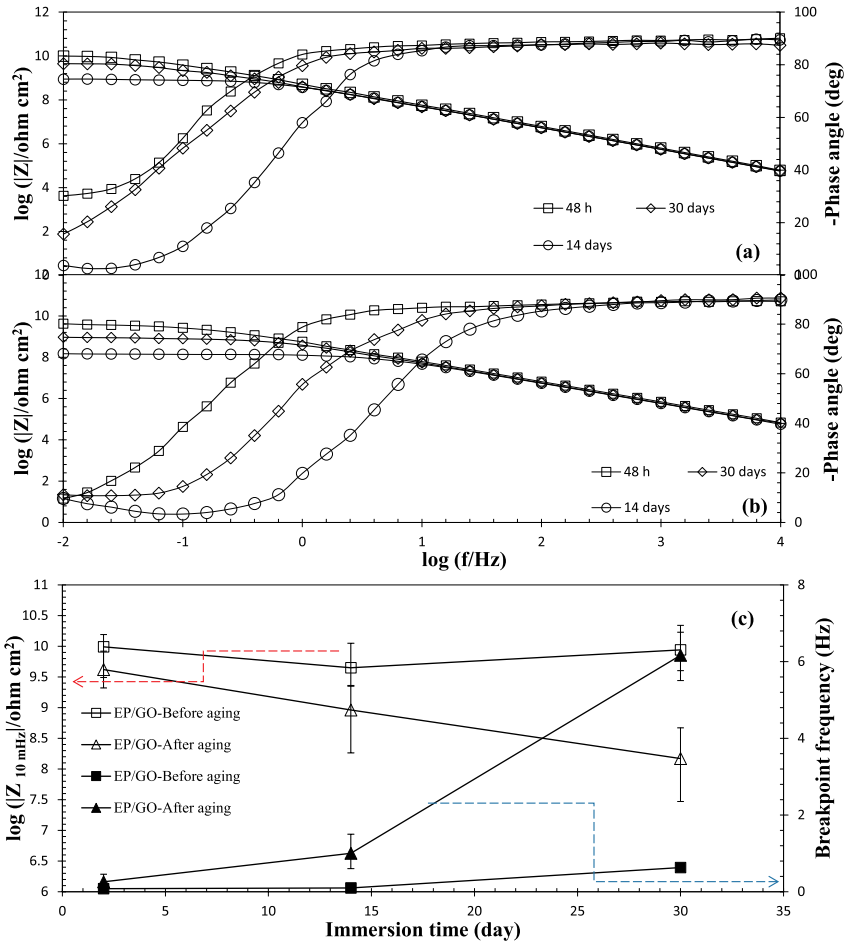

Fig. 11. Bode diagrams of Epoxy/GO samples exposed to 3.5 wt% NaCl solution for 30 days, (a) before QUV aging and (b) after 300 h QUV aging; (c) the plots of Z10 mHz and breakpoint frequency versus the time of immersion.

GO-PANI/Epoxy coatings thanks to its even surface before exposure and its high level of weathering stability during weathering cycles. These results are confirming the results obtained from gonio-spectrophotometry and contact angle measurements.

3.2.3. *Thermo-mechanical properties (DMTA)*

So far, the improved weathering stability of epoxy coating in presence of graphene oxide and especially PANI-modified graphene oxide has been demonstrated by various techniques. The overall network structure of various coatings and their variations during weathering should be considered. For such purpose, physical/mechanical properties of coatings were investigated by DMTA technique. In Fig. 9, the Tan δ and storage modulus versus temperature before and after weathering are plotted for different samples. The parameters of glass transition temperature (T_g), cross-linking density (ϑ_e) and peak width are calculated from Fig. 9 and presented in Table 2. The following equation has been used to calculate the cross-linking density.

$$\vartheta_e = \frac{E'}{3RT}$$

In this equation, E' and T are respectively the storage modulus and corresponded temperature at beginning of plateau rubbery region, and R is universal Gas constant.

As shown in Table 2, the highest cross-linking density before weathering was observed for Neat Epoxy sample. The lower crosslinking density in other samples may be attributed to the hindrance effects of GO and GO-PANI on the curing reactions of epoxy. Such plate-like nanofillers which are vastly dispersed within polymeric chains can directly obstruct the curing reactions between epoxy and hardener [60–62]. On the other hands, these nanofillers indirectly affect the curing process via their influence on viscosity. The high surface area of these nanostructures considerably increases their physical interaction with epoxy chains, leading to a significant increase in viscosity. Increased viscosity and consequent reduced mobility of the chains results in a less efficient curing process and therefore, reduced crosslinking density and more unreacted functional groups remained in the coating.

The variations in cross-linking density after weathering reveal that Neat epoxy and filled epoxies behave differently during weathering. While the Neat Epoxy experiences a drop in cross-linking density, the filled epoxies (GO/Epoxy and GO-PANI/Epoxy) encounter with a slight increase in cross-linking density. Such different behavior can be explained by their initial specific structure (before weathering) and the competition of weathering degradation and post curing reactions at initial stage of weathering.

The less cross-linked network of GO/Epoxy and GO-PANI/Epoxy compared to the Neat Epoxy reflects their immature network. Such immaturity before weathering exposure can be a latent potential for post-curing reactions during weathering. According to the slight increase in cross-linking density values after weathering for GO/Epoxy and GO-PANI/Epoxy samples, it can be proposed that the remained unreacted groups on polymeric structures can partially react and form new crosslinking during weathering (post-curing). The occurrence of post curing reactions (which promote the cross-linking density) and its competition with weathering degradation (which reduces the cross-linking density) have been investigated in various thermosetting systems [56,58,61]. For high cross-linked network of Neat epoxy which is

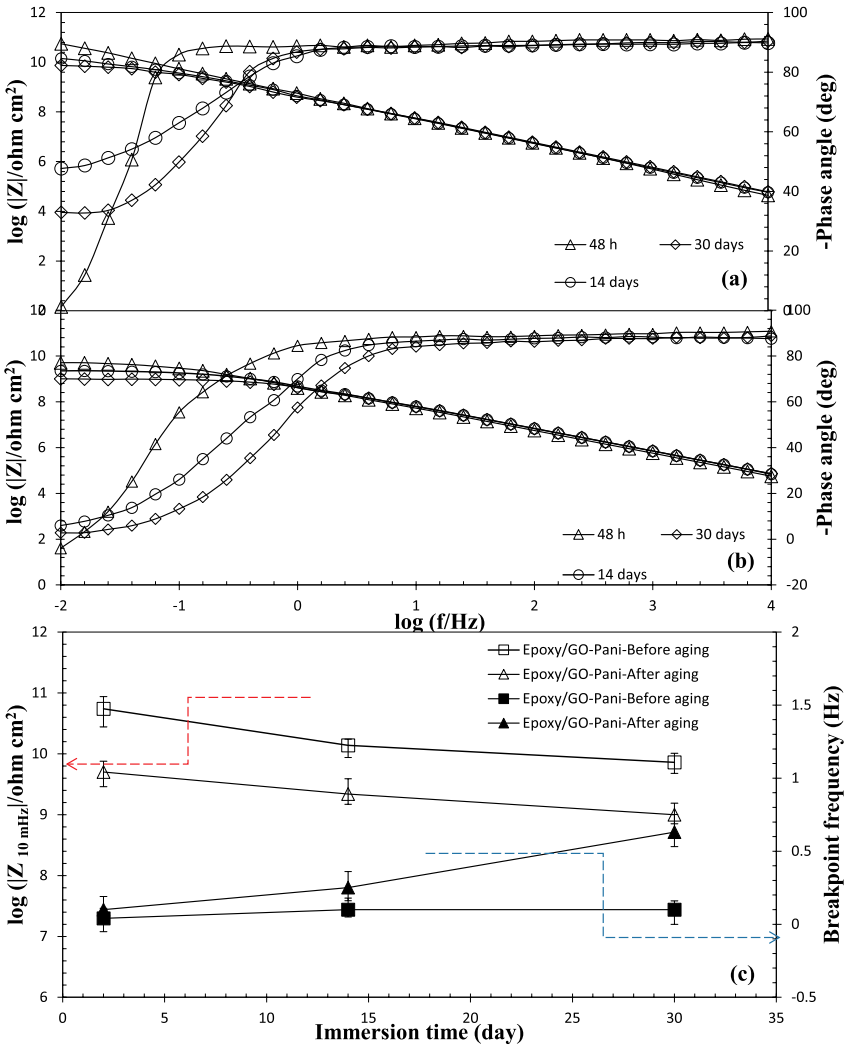

Fig. 12. Bode diagrams of Epoxy/GO-PANI samples exposed to 3.5 wt% NaCl solution for 30 days, (a) before QUV aging and (b) after 300 h QUV aging;; (c) the plots of Z10 mHz and breakpoint frequency versus the time of immersion.

considered as a mature network, the chance of post curing reactions is significantly reduced. According to the previous results, this coating experiences the highest level of weathering degradation. Therefore, the low chance of post curing reactions together with the high level of weathering degradation in Neat epoxy makes it susceptible for dominancy of weathering degradation, leading to a reduction in crosslinking density. On the other hands, for the immature network of filled epoxies, the chance of post curing is higher and simultaneously they tolerate much less degradation thank to the high level of protection in presence of pristine and modified graphene oxide. In these networks, the post curing reactions become dominant and results in an increase in cross-linking density after 300 h weathering exposure.

Table 2 also reveals the glass transition temperature (T_g) and peak width of various coatings during weathering. In general, it is observed that for all coatings, both parameters increases during weathering which can be assigned to the well-known phenomena (hardening effect and decreased homogeneity) during weathering [63]. Interestingly, the much lower peak width for GO-PANI/Epoxy compared to other samples can again reflect the high homogeneity and compatibility between GO-PANI and epoxy system.

Finally, it should be clarified that lower crosslinking density of filled epoxies should not be considered as a main concern. It is because of this fact that epoxy systems are usually known as high cross-linked networks. The high level of crosslinking in some applications is regarded as a drawback since it causes too much fragility in the network. Therefore, adjusting the crosslinking density can be desired provided that the main functions of the coating not be negatively affected. Surprisingly, in case of epoxy coating studied here, the short- and long-term properties (already investigated by different techniques) and also corrosion performance (which will be studied in the next section) revealed that such scarified crosslinking density in GO/Epoxy and GO-PANI systems not only has not negatively affected their main functions, but also has resulted in a superior performance in weathering and corrosion performance of the coatings.

3.3. Corrosion studies

3.3.1. EIS test results

The preventative effect of GO and polyaniline on the epoxy coating photo-degradation through absorbing and/or scattering the UV light during weathering time on its corrosion preventative ability was studied by EIS and salt spray test. Bode plots are provided for the weathered and un-weathered neat epoxy, epoxy/GO and epoxy/GO-PANI samples after 2, 14 and 30 days immersion in chloride solution (Figs. 10–12).

To analyze the EIS test results the values of low frequency impedance (|Z| at 10 mHz) and breakpoint frequency (f_b) were extracted from Bode diagrams and are presented in a plot as a function of immersion time. All plots reveal a descending trend as function of immersion time progress

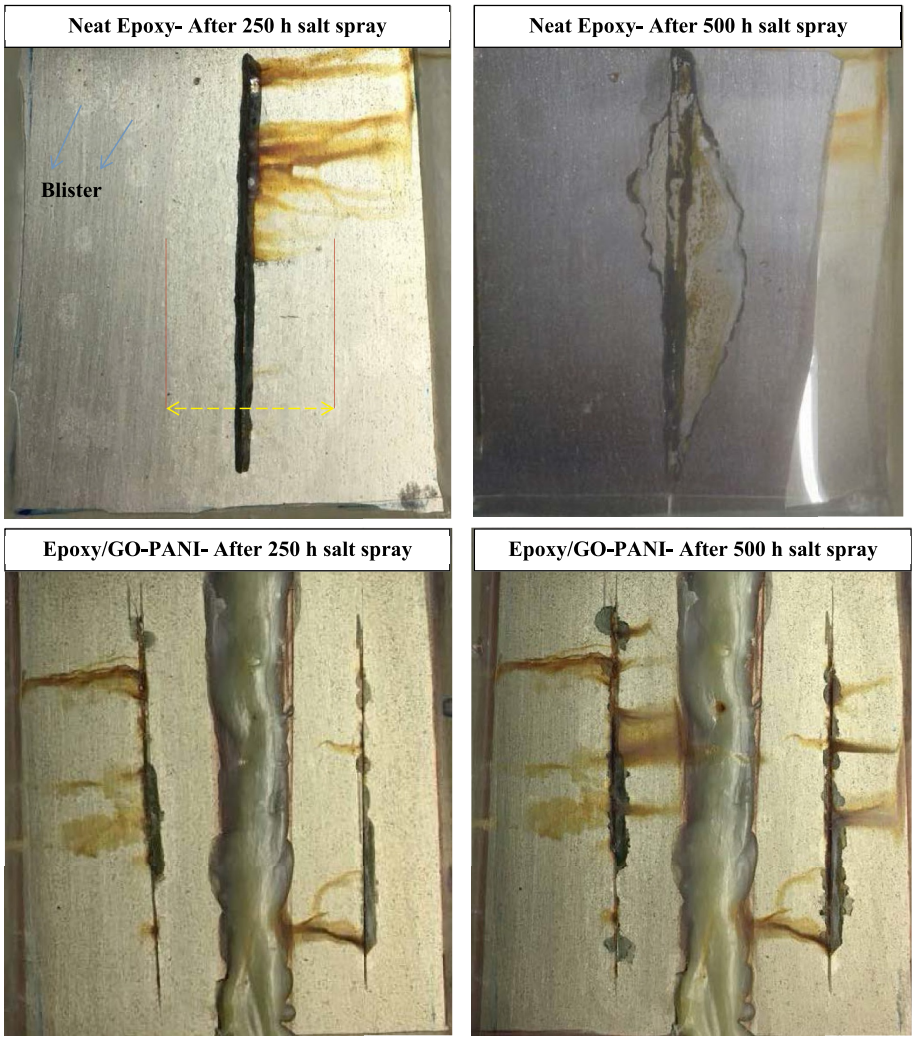

Fig. 13. Salt spray test results for the previously weathered samples (for 300 h QUV aging) after 250 and 500 h salt spray exposure.

for all samples. Bode diagrams of the un-weathered GO-PANI loaded sample shows capacitive response in the wide frequency range, $|Z|_{at\ 10\ mHz} > 10^{10}\ \Omega\ cm^2$ and the high frequency phase angle ($\Theta_{10\ kHz}$) of almost $-90°$. It is clear from the results that at all immersion time the GO-PANI loaded sample shows much greater $|Z|_{at\ 10\ mHz}$, revealing that the PANI deposition on the GO sheets promoted its power in the coating corrosion preventative capability. The excellently improved barrier performance of the epoxy against water and ions diffusion may be explained by two major mechanisms. First, the PANI deposition over the GO sheets provides a hydrophobic surface impermeable to water. There are some unwilled defects in the structure of GO that may be generated during oxidation of graphite. These defects are large enough to weaken the barrier properties of GO [64]. PANI film deposited on the GO sheets fills the defect sites and promotes their barrier properties. Second, the PANI layer deposition on the GO sheets help us to gain higher degree of nanosheets exfoliation in polymer matrix due to the role of PANI in nanosheets interlayer distance and stability in polymer matrix. Upon exposure and the corrosive electrolyte diffusion into the epoxy matrix, the coating degradation happens, leading to loss of barrier action. It seems that in the presence of GO-PANI the coating barrier properties and therefore resistance against degradation in corrosive electrolyte can be significantly improved. PANI also plays another important role in the coating anti-corrosion properties promotion. According to literature PANI can increase the local pH beneath the coating on the anodic sites of metal substrate, providing the condition for conversion of Fe^{2+} to Fe^{3+} and formation of passive Fe_2O_3 layer on the metal surface [65]. The effect of QUV aging on the protection performance of the epoxy coatings with and without nanoparticles was studied by EIS (Figs. 10–12). Fig. 10 shows significant decrease in $|Z|_{at\ 10\ mHz}$ and increase in f_b for the neat epoxy sample aged in the QUV condition. This means that the barrier properties of the neat epoxy sample significantly decreases in UV condition. This is attributed to the significant decrease in the cross-linking density of the epoxy coating resulted by photo-degradation. The lowest decrease in $|Z|_{at\ 10\ mHz}$ and increase in f_b after weathering were observed for the Epoxy/GO-PANI sample, reflecting the lowest barrier properties decline. The role of GO-PANI in restriction of water diffusion into coating matrix and its high UV shielding capability are the main causes of lower coating protective performance decline. The excellent antioxidant natures of the GO-PANI composite are responsible for the coating degradation prevention and lower barrier properties decline. On the other hand, the neat GO could not provide promising protection behaviors against UV irradiation and water permeation. This means that deposition of PANI on GO could provide a multifunctional composite with excellent barrier and UV blocking behaviors. The effective role of GO-PANI nanosheets in the water/humidity, oxygen and corrosive species penetration length and time is the reason for postponing the hydrolytic degradation and promoting the corrosion resistance of the coating after QUV exposure.

3.3.2. *Salt spray test results*

The anti-corrosion properties of the Neat epoxy and GO-PANI loaded coatings subjected to QUV aging condition for 300 h were also examined

by salt spray test. In agreement with EIS test results the poor anti-corrosion properties of the Neat epoxy sample is also obvious from salt spray test results. Fig. 13 declares significant coating displacement from the substrate around scratch and blistering on the intact parts of the neat epoxy sample. This is a sign for the huge electrolyte diffusion into coating/metal interface, corrosion reactions progress and adhesion bonds damage. This observation clarifies that neat epoxy sample was severely aged in the QUV test condition, leading to the barrier function loss and interfacial adhesion bonds weakening. In fact, the coating compactness and cross-linking density can be drastically affected as a result of photo-degradation, leading to defects creation and barrier activity decline. On the other hand, the corrosion products progress on the GO-PANI loaded sample is limited only to the scratch part. There is almost no corrosion spot and delaminated part on the intact part of the coating, meaning that the high barrier performance of the coating has not been changed even after 300 h exposure to QUV test condition. This observation further shows the impact of GO-PANI particles on UV and humidity shielding effect, protecting the coating from severe aging in QUV test. These observations again reveal that inclusion of GO-PANI sheets into the epoxy matrix could provide high resistance against UV aging and promote the coating protection function through limiting the degradation extent.

4. Conclusion

A layer of polyaniline was polymerized over graphene oxide by an in-situ process. The Successful deposition of a polyaniline over modified nanosheets (GO-PANI) was approved with FTIR, XRD, Raman, UV–Visible and FE-SEM analyses. The DPPH assay results revealed that a considerable improvement (more than five times) in radical scavenging capabilities of graphene oxide was achieved in presence of polyaniline. The GO and GO-PANI were then employed to increase the weathering and corrosion properties of epoxy coatings. The weathered and corroded epoxy coatings were evaluated by different approaches. The results clearly depicted a high level of protection against weathering and corrosion has been achieved in presence of GO-PANI. It was finally concluded that such improvement can be accounted for by different modes of action of GO-PANI during weathering and corrosion cycles. Beside the positive impact of polyaniline on dispersion of graphene oxide within epoxy matrix, the cooperation of graphene oxide and polyaniline in enhancing UV shielding, radical scavenging and barrier properties was the main mechanism involved in simultaneous promotion of weathering and corrosion performance.

References

[1] Yari H, Moradian S, Tahmasebi N. The weathering performance of acrylic melamine automotive clearcoats containing hydrophobic nanosilica. J Coat Technol Res 2014;11. https://doi.org/10.1007/s11998-013-9541-z.

[2] Razin AA, Yari H, Ramezanzadeh B. Stone-chipping and adhesion deterioration of automotive coating systems caused by outdoor weathering of underneath layers. J Ind Eng Chem 2015;31:291–300. https://doi.org/10.1016/j.jiec.2015.07.001.

[3] Rashvand M, Ranjbar Z, Rastegar S. Nano zinc oxide as a UV-stabilizer for aromatic polyurethane coatings. Prog Org Coating 2011;71:362–8. https://doi.org/10.1016/j.porgcoat.2011.04.006.

[4] Cristea MV, Riedl B, Blanchet P. Effect of addition of nanosized UV absorbers on the physico-mechanical and thermal properties of an exterior waterborne stain for wood. Prog Org Coating 2011;72:755–62. https://doi.org/10.1016/j.porgcoat.2011.08.007.

[5] Pakravan HR, Yari H. The influence of nanostructured UV-blockers on mechanical properties of carbon fiber epoxy composites during accelerated weathering condition. Polym Adv Technol 2018;29. https://doi.org/10.1002/pat.4208.

[6] Ghazi A, Ghasemi E, Mahdavian M, Ramezanzadeh B, Rostami M. The application of benzimidazole and zinc cations intercalated sodium montmorillonite as smart ion exchange inhibiting pigments in the epoxy ester coating. Corros Sci 2015;94:207–17. https://doi.org/10.1016/J.CORSCI.2015.02.007.

[7] Alibakhshi E, Ghasemi E, Mahdavian M, Ramezanzadeh B. Corrosion inhibitor release from Zn-Al-[PO 4 3-]-[CO 3 2-] layered double hydroxide nanoparticles, vol. 9; 2016. p. 233–48.

[8] Hasani M, Mahdavian M, Yari H, Ramezanzadeh B. Versatile protection of exterior coatings by the aid of graphene oxide nano-sheets; comparison with conventional UV absorbers. Prog Org Coating 2017. https://doi.org/10.1016/j.porgcoat.2017.11.020.

[9] Nuraje N, Khan SI, Misak H, Asmatulu R. The addition of graphene to polymer coatings for improved weathering. ISRN Polym Sci 2013;2013:1–8. https://doi.org/10.1155/2013/514617.

[10] Alhumade H, Yu A, Elkamel A, Simon AA L. Enhanced protective properties and UV stability of epoxy/graphene nanocomposite coating on stainless steel. Express Polym Lett 2016;10:1034–46.

[11] Mohan VB, Lau K, Hui D, Bhattacharyya D. Graphene-based materials and their composites: a review on production, applications and product limitations. Compos B Eng 2018;142:200–20. https://doi.org/10.1016/J.COMPOSITESB.2018.01.013.

[12] Ahmad H, Fan M, Hui D. Graphene oxide incorporated functional materials: a review. Compos B Eng 2018;145:270–80. https://doi.org/10.1016/J.COMPOSITESB.2018.02.006.

[13] Shi Y-C, Feng J-J, Lin X-X, Zhang L, Yuan J, Zhang Q-L, et al. One-step hydrothermal synthesis of three-dimensional nitrogen-doped reduced graphene oxide hydrogels anchored PtPd alloyed nanoparticles for ethylene glycol oxidation and hydrogen evolution reactions. Electrochim Acta 2019;293:504–13. https://doi.org/10.1016/J.ELECTACTA.2018.10.068.

[14] Zhu X-Y, Lv Z-S, Feng J-J, Yuan P-X, Zhang L, Chen J-R, et al. Controlled fabrication of well-dispersed AgPd nanoclusters supported on reduced graphene oxide with highly enhanced catalytic properties towards 4-nitrophenol reduction. J Colloid Interface Sci 2018;516:355–63. https://doi.org/10.1016/J.JCIS.2018.01.047.

[15] Zhang X-F, Zhu X-Y, Feng J-J, Wang A-J. Solvothermal synthesis of N-doped graphene supported PtCo nanodendrites with highly catalytic activity for 4-nitrophenol reduction. Appl Surf Sci 2018;428:798–808. https://doi.org/10.1016/J.APSUSC.2017.09.200.

[16] Meriga V, Valligatla S, Sundaresan S, Cahill C, Dhanak VR, Chakraborty AK. Optical, electrical, and electrochemical properties of graphene based water soluble polyaniline composites. J Appl Polym Sci 2015;132. https://doi.org/10.1002/app.42766. n/a-n/a.

[17] Lebegue S, Klintenberg M, Eriksson O, Katsnelson MI. Accurate electronic band gap of pure and functionalized graphane from GW calculations. 2009. https://doi.org/10.1103/PhysRevB.79.245117.

[18] Tissera ND, Wijesena RN, Perera JR, de Silva KMN, Amaratunge GAJ. Hydrophobic cotton textile surfaces using an amphiphilic graphene oxide (GO) coating. Appl Surf Sci 2015;324:455–63. https://doi.org/10.1016/J.APSUSC.2014.10.148.

[19] Ouadil B, Cherkaoui O, Safi M, Zahouily M. Surface modification of knit polyester fabric for mechanical, electrical and UV protection properties by coating with graphene oxide, graphene and graphene/silver nanocomposites. Appl Surf Sci 2017;414:292–302. https://doi.org/10.1016/J.APSUSC.2017.04.068.

[20] Tang X, Tian M, Qu L, Zhu S, Guo X, Han G, et al. Functionalization of cotton fabric with graphene oxide nanosheet and polyaniline for conductive and UV blocking properties. Synth Met 2015;202:82–8. https://doi.org/10.1016/J.SYNTHMET.2015.01.017.

[21] Qiu Y, Wang Z, Owens ACE, Kulaots I, Chen Y, Kane AB, et al. Antioxidant chemistry of graphene-based materials and its role in oxidation protection technology. Nanoscale 2014;6:11744–55. https://doi.org/10.1039/c4nr03275f.

[22] Xia W, Zhao J, Wang T, Song L, Gong H, Guo H, et al. Anchoring ceria nanoparticles on graphene oxide and their radical scavenge properties under gamma irradiation environment. Phys Chem Chem Phys 2017;19:16785–94. https://doi.org/10.1039/C7CP02559A.

[23] Yang J, Huang Y, Lv Y, Zhao P, Yang Q, Li G, et al. The intrinsic thermal-oxidative stabilization effect of chemically reduced graphene oxide on polypropylene. J Mater Chem 2013;1:11184. https://doi.org/10.1039/c3ta11989k.

[24] Ramezanzadeh B, Ghasemi E, Mahdavian M, Changizi E. Covalently-grafted graphene oxide nanosheets to improve barrier and corrosion protection properties of polyurethane coatings. Carbon N Y 2015;93:555–73. https://doi.org/10.1016/j.carbon.2015.05.094.

[25] Ramezanzadeh B, Haeri Z, Ramezanzadeh M. A facile route of making silica nanoparticles-covered graphene oxide nanohybrids (SiO2-GO); fabrication of SiO2-GO/epoxy composite coating with superior barrier and corrosion protection performance. Chem Eng J 2016;303:511–28. https://doi.org/10.1016/j.cej.2016.06.028.

[26] Di H, Yu Z, Ma Y, Zhang C, Li F, Lv L, et al. Corrosion-resistant hybrid coatings based on graphene oxide–zirconia dioxide/epoxy system. J Taiwan Inst Chem Eng 2016;67:511–20. https://doi.org/10.1016/J.JTICE.2016.08.008.

[27] Daradmare S, Raj S, Bhattacharyya AR, Parida S. Factors affecting barrier performance of composite anti-corrosion coatings prepared by using electrochemically exfoliated few-layer graphene as filler. Compos B Eng 2018;155:1–10. https://doi.org/10.1016/J.COMPOSITESB.2018.08.023.

[28] Miraftab R, Ramezanzadeh B, Bahlakeh G, Mahdavian M. An advanced approach for fabricating a reduced graphene oxide-AZO dye/polyurethane composite with enhanced ultraviolet (UV) shielding properties: experimental and first-principles QM modeling. Chem Eng J 2017;321:159–74. https://doi.org/10.1016/j.cej.2017.03.124.

[29] Mahdavian M, Yari H, Ramezanzadeh B, Bahlakeh G, Hasani M. Immobilization of ultraviolet absorbers on graphene oxide nanosheets to be utilized as a multifunctional hybrid UV-blocker: a combined density functional theory and practical application. Appl Surf Sci 2018;447. https://doi.org/10.1016/j.apsusc.2018.03.211.

[30] Ramezanzadeh M, Asghari M, Ramezanzadeh B, Bahlakeh G. Fabrication of an efficient system for Zn ions removal from industrial wastewater based on graphene oxide nanosheets decorated with highly crystalline polyaniline nanofibers (GO-

PANI): experimental and ab initio quantum mechanics approaches. Chem Eng J 2018;337:385–97. https://doi.org/10.1016/J.CEJ.2017.12.102.
[31] Ramezanzadeh B, Mohamadzadeh Moghadam MH, Shohani N, Mahdavian M. Effects of highly crystalline and conductive polyaniline/graphene oxide composites on the corrosion protection performance of a zinc-rich epoxy coating. Chem Eng J 2017;320:363–75. https://doi.org/10.1016/j.cej.2017.03.061.
[32] Ramezanzadeh B, Kardar P, Bahlakeh G, Hayatgheib Y, Mahdavian M. Fabrication of a highly tunable graphene oxide composite through layer-by-layer assembly of highly crystalline polyaniline nanofibers and green corrosion inhibitors: complementary experimental and first-principles quantum-mechanics modeling approaches. J Phys Chem C 2017;121:20433–50. https://doi.org/10.1021/acs.jpcc.7b04323.
[33] Hayatgheib Y, Ramezanzadeh B, Kardar P, Mahdavian M. A comparative study on fabrication of a highly effective corrosion protective system based on graphene oxide-polyaniline nanofibers/epoxy composite. Corros Sci 2018;133:358–73. https://doi.org/10.1016/J.CORSCI.2018.01.046.
[34] Bai H, Xu Y, Zhao L, Li C, Shi G. Non-covalent functionalization of graphene sheets by sulfonated polyaniline. Chem Commun 2009;0:1667. https://doi.org/10.1039/b821805f.
[35] Hu F, Li W, Zhang J, Meng W. Effect of graphene oxide as a dopant on the electrochemical performance of graphene oxide/polyaniline composite. J Mater Sci Technol 2014;30:321–7. https://doi.org/10.1016/J.JMST.2013.10.009.
[36] Razin AA, Yari H, Ramezanzadeh B. Stone-chipping and adhesion deterioration of automotive coating systems caused by outdoor weathering of underneath layers. J Ind Eng Chem 2015;31. https://doi.org/10.1016/j.jiec.2015.07.001.
[37] Alizadeh Razin A, Ramezanzadeh B, Yari H. Detecting and estimating the extent of automotive coating delamination and damage indexes after stone chipping using electrochemical impedance spectroscopy. Prog Org Coating 2015. https://doi.org/10.1016/j.porgcoat.2015.11.023.
[38] Yan X, Chen J, Yang J, Xue Q, Miele P. Fabrication of free-standing, electrochemically active, and biocompatible graphene Oxide−Polyaniline and Graphene−Polyaniline hybrid papers. ACS Appl Mater Interfaces 2010;2:2521–9. https://doi.org/10.1021/am100293r.
[39] McLAREN K. XIII-the development of the CIE 1976 (L* a* b*) uniform colour space and colour-difference formula. J Soc Dye Colour 2008;92:338–41. https://doi.org/10.1111/j.1478-4408.1976.tb03301.x.
[40] Musico YLF, Santos CM, Dalida MLP, Rodrigues DF. Improved removal of lead(ii) from water using a polymer-based graphene oxide nanocomposite. J Mater Chem 2013;1:3789–96. https://doi.org/10.1039/c3ta01616a.
[41] Zhang F, Wang B, He S, Man R. Preparation of graphene-oxide/polyamidoamine dendrimers and their adsorption properties toward some heavy metal ions. J Chem Eng Data 2014;59:1719–26. https://doi.org/10.1021/je500219e.
[42] Zhang WL, Park BJ, Choi HJ. Colloidal graphene oxide/polyaniline nanocomposite and its electrorheology. Chem Commun 2010;46:5596. https://doi.org/10.1039/c0cc00557f.
[43] Athawale AA, Kulkarni MV, Chabukswar VV. Studies on chemically synthesized soluble acrylic acid doped polyaniline. Mater Chem Phys 2002;73:106–10. https://doi.org/10.1016/S0254-0584(01)00338-8.
[44] Mitra M, Kulsi C, Chatterjee K, Kargupta K, Ganguly S, Banerjee D, et al. Reduced graphene oxide-polyaniline composites—synthesis, characterization and optimization for thermoelectric applications. RSC Adv 2015;5:31039–48. https://doi.org/10.1039/C5RA01794G.
[45] Chaudhari HK, Kelkar DS. Investigation of structure and electrical conductivity in doped polyaniline. Polym Int 1997;42:380–4. https://doi.org/10.1002/(SICI)1097-0126(199704)42:4<380. AID-PI727>3.0.CO;2-F.
[46] Pouget JP, Jozefowicz ME, Epstein AJ, Tang X, MacDiarmid AG. X-ray structure of polyaniline. Macromolecules 1991;24:779–89. https://doi.org/10.1021/ma00003a022.
[47] Tuinstra F, Koenig JL. Raman spectrum of graphite. J Chem Phys 1970;53:1126–30. https://doi.org/10.1063/1.1674108.
[48] Pimenta MA, Dresselhaus G, Dresselhaus MS, Cançado LG, Jorio A, Saito R. Studying disorder in graphite-based systems by Raman spectroscopy. Phys Chem Chem Phys 2007;9:1276–90. https://doi.org/10.1039/B613962K.
[49] Liu L, Li C, Bao C, Jia Q, Xiao P, Liu X, et al. Preparation and characterization of chitosan/graphene oxide composites for the adsorption of Au(III) and Pd(II). Talanta 2012;93:350–7. https://doi.org/10.1016/J.TALANTA.2012.02.051.
[50] Fan L, Luo C, Sun M, Qiu H. Synthesis of graphene oxide decorated with magnetic cyclodextrin for fast chromium removal. J Mater Chem 2012;22:24577. https://doi.org/10.1039/c2jm35378d.
[51] Kou L, Gao C. Making silicananoparticle-covered graphene oxide nanohybrids as general building blocks for large-area superhydrophilic coatings. Nanoscale 2011;3:519–28. https://doi.org/10.1039/C0NR00609B.
[52] Lee CY, Bae J-H, Kim T-Y, Chang S-H, Kim SY. Using silane-functionalized graphene oxides for enhancing the interfacial bonding strength of carbon/epoxy composites. Compos Part A Appl Sci Manuf 2015;75:11–7. https://doi.org/10.1016/J.COMPOSITESA.2015.04.013.
[53] Yari H, Moradian S, Tahmasebi N, Arefmanesh M. The effect of weathering on tribological properties of an acrylic melamine automotive nanocomposite. Tribol Lett 2012;46:123–30.
[54] Nguyen T, Martin J, Byrd E, Embree N. Relating laboratory and outdoor exposure of coatingsIII. Effect of relative humidity on moisture-enhanced photolysis of acrylic-melamine coatings. Polym Degrad Stabil 2002;77:1–16. https://doi.org/10.1016/S0141-3910(02)00070-8.
[55] Alizadeh Razin A, Ramezanzadeh B, Yari H. Detecting and estimating the extent of automotive coating delamination and damage indexes after stone chipping using electrochemical impedance spectroscopy. Prog Org Coating 2016;92:95–109. https://doi.org/10.1016/j.porgcoat.2015.11.023.
[56] Rafiei R, Mohseni M, Yari H, Mahdavi M. Evaluation of degradability of two polyurethane refinish coatings against biological materials: a case study. Prog Org Coating 2016;93. https://doi.org/10.1016/j.porgcoat.2015.12.012.
[57] Yang X, Vang C Tallman D, Bierwagen G, Croll S, Rohlik S. Weathering degradation of a polyurethane coating. Polym Degrad Stabil 2001;74:341–51. https://doi.org/10.1016/S0141-3910(01)00166-5.
[58] Osterhold M, Gl, ckner P. Influence of weathering on physical properties of clearcoats. Prog Org Coating 2001;41:177–82. https://doi.org/10.1016/S0300-9440(01)00152-7.
[59] Yari H, Moradian S, Ramezanzadeh B, Kashani A, Niknahad M. The influence of basecoat pigmentation on chemical structure and surface topology of automotive clearcoats during weathering. Prog Org Coating 2012;75:420–8.
[60] Yari H, Mohseni M, Ranjbar Z. Thermomechanical and chemorheology properties of a thermosetting acrylic/melamine clearcoat modified with a hyperbranched polymer. J Appl Polym Sci 2013;129:1929–38. https://doi.org/10.1002/app.38886.
[61] Yari H, Moradian S, Tahmasebi N, Arefmanesh M. The effect of weathering on tribological properties of an acrylic melamine automotive nanocomposite. Tribol Lett 2012;46:123–30. https://doi.org/10.1007/s11249-012-9928-5.
[62] Yari H, Mohseni M. Curing and thermo-mechanical studies of a modified thermosetting clearcoat containing OH-functional POSS nanocages. Prog Org Coating 2015;87:129–37. https://doi.org/10.1016/j.porgcoat.2015.05.024.
[63] Yari H, Moradian S, Ramazanzade B, Kashani A, Tahmasebi N. The effect of basecoat pigmentation on mechanical properties of an automotive basecoat/clearcoat system during weathering. Polym Degrad Stabil 2009;94:1281–9. https://doi.org/10.1016/j.polymdegradstab.2009.04.008.
[64] Tian W, Li W, Yu W, Liu X, Tian W, Li W, et al. A review on lattice defects in graphene: types, generation, effects and regulation. Micromachines 2017;8:163. https://doi.org/10.3390/mi8050163.
[65] Yi Yuetao, Liu Guangyang, Zhiming Jin DF. The use of conducting polyaniline as corrosion inhibitor for mild steel in hydrochloric acid. Int J Electrochem Sci 2013;8:3540–50.